ORIGINAL ARTICLE

Longitudinal motor system changes from acute to chronic spinal cord injury

Tim M. Emmenegger[1] | Dario Pfyffer[1,2] | Armin Curt[1] |
Simon Schading-Sassenhausen[1] | Markus Hupp[1] | John Ashburner[3] | Karl Friston[3] |
Nikolaus Weiskopf[4,5] | Alan Thompson[6] | Patrick Freund[1,3,4]

[1]Spinal Cord Injury Centre, Balgrist University Hospital, University of Zurich, Zurich, Switzerland

[2]Systems Neuroscience and Pain Lab, Department of Anesthesiology, Perioperative and Pain Medicine, Stanford University School of Medicine, Palo Alto, California, USA

[3]Wellcome Trust Centre for Neuroimaging, Queen Square Institute of Neurology, University College London, London, UK

[4]Department of Neurophysics, Max Planck Institute for Human Cognitive and Brain Sciences, Leipzig, Germany

[5]Felix Bloch Institute for Solid State Physics, Faculty of Physics and Earth Sciences, Leipzig University, Leipzig, Germany

[6]Queen Square Multiple Sclerosis Centre, Institute of Neurology, University College London, London, UK

Correspondence
Patrick Freund, Spinal Cord Injury Centre, Balgrist University Hospital, University of Zurich, Forchstrasse 380, 8008 Zurich, Switzerland.
Email: patrick.freund@balgrist.ch

Abstract

Background and purpose: In acute spinal cord injury (SCI), magnetic resonance imaging (MRI) reveals tissue bridges and neurodegeneration for 2 years. This 5-year study aims to track initial lesion changes, subsequent neurodegeneration, and their impact on recovery.

Methods: This prospective longitudinal study enrolled acute SCI patients and healthy controls who were assessed clinically—and by MRI—regularly from 3 days postinjury up to 60 months. We employed histologically cross-validated quantitative MRI sequences sensitive to volume, myelin, and iron changes, thereby reflecting indirectly processes of neurodegeneration and neuroinflammation. General linear models tracked lesion and remote changes in volume, myelin- and iron-sensitive magnetic resonance indices over 5 years. Associations between lesion, degeneration, and recovery (using the Spinal Cord Independence Measure [SCIM] questionnaire and the International Standards for Neurological Classification of Spinal Cord Injury total motor score) were assessed.

Results: Patients' motor scores improved by an average of 12.86 (95% confidence interval [CI] = 6.70–19.00) points, and SCIM by 26.08 (95% CI = 17.00–35.20) points. Within 3–28 days post-SCI, lesion size decreased by more than two-thirds (3 days: 302.52 ± 185.80 mm^2, 28 days: 76.77 ± 88.62 mm^2), revealing tissue bridges. Cervical cord and corticospinal tract volumes transiently increased in SCI patients by 5% and 3%, respectively, accompanied by cervical myelin decreases and iron increases. Over time, progressive atrophy was observed in both regions, which was linked to early lesion dynamics. Tissue bridges, reduced swelling, and myelin content decreases were predictive of long-term motor score recovery and improved SCIM score.

Conclusions: Studying acute changes and their impact on longer follow-up provides insights into SCI trajectory, highlighting the importance of acute intervention while indicating the potential to influence outcomes in the later stages.

KEYWORDS
acute spinal cord injury, iron, lesion core, MRI, neurodegeneration

INTRODUCTION

Spinal cord injury (SCI), for which there is no cure, usually results in incomplete recovery [1]. Initial cord damage at the site of the lesion is followed by remote and progressive degenerative changes [2]. Current clinical evaluation is focused on the extent of the initial cord damage by means of clinical impairment scores and electrophysiological properties of major spinal pathways, but does not include remote neurodegeneration. These neurodegenerative processes—which are known to progress for at least 2 years post-injury [3]—are likely to have a negative impact on the recovery potential. Hence, there is a pressing need to understand over which period these neurodegenerative changes continue and to define their relationship with early local cord pathology and their clinical relevance. A better understanding of these interrelated pathophysiological processes could offer important insights into individually focused treatment, not only in the acute, but also in the chronic phase of SCI.

Advances in quantitative magnetic resonance imaging (MRI), combined with a new anatomical template covering both brain and cervical cord (C1–C3) [4], provide an unprecedented opportunity to noninvasively estimate myelin, iron, and volume changes of grey matter (GM) and white matter (WM) across the neuraxis. By extending the previous 2-year follow-up study to 5 years [3], we aimed to (i) establish the hyperacute dynamics of the evolving focal lesion, (ii) characterize the trajectories of neurodegenerative changes in the spinal cord and brain over 5 years post-SCI, (iii) clarify how local lesion changes drive remote neurodegeneration, and (iv) explore how these changes impact patients' recovery potential. To this end, we quantified the hyperacute evolution of the lesion (via T2-weighted [T2w] scans) and changes in volume (via T1w scans), and myelin-sensitive (via magnetization transfer saturation [MT_{sat}] [5, 6]) and iron-sensitive (via effective transverse relaxation rate [R2*] [5]) metrics in the brain and cervical cord [2].

MATERIALS AND METHODS

Participants and study design

We recruited consecutively acute (≤1 month) SCI patients at Balgrist University Hospital (Zurich, Switzerland) between September 2010 and June 2018; some of these data were reported during the first 2 years post-SCI (Table 1) [3, 7]. At every visit (3 days and 1, 3, 6, 12, 24, and 60 months postinjury), individuals with SCI underwent clinical evaluation, including the International Standards for Neurological Classification of Spinal Cord Injury [8] motor scores and the Spinal Cord Independence Measure (SCIM) [9], ranging from 0 (full impairment) to 100 (no impairment). All participants underwent standard clinical care at Balgrist University Hospital, and specific information regarding their hospitalization duration can be found in Table 1. Two patients died from a cause unrelated to SCI (Figure S1.1). Healthy controls from the local area followed the same schedule as the patients. All participants were older than 18 years and had no pre-existing neurological, mental, or medical disorders, no brain lesions on MRI, and no contraindications to MRI. We included both traumatic and also nontraumatic SCI patients (see Table 1), as there is no clear evidence that these show differences in the recovery profiles or differences in the focal lesion dynamics [10–12]. The study was approved by the local ethics committee of Zurich (KEK-ZH, EK-2010-0271 and PB_2016-00230) and was in accordance with the Declaration of Helsinki, and all participants gave informed written consent.

Procedures

For the hyperacute scan of the focal lesion, a conventional T2w sequence on 1.5T or 3T (Philips Achieva [Philips Healthcare], Siemens Magnetom Verio, Skyra^fit, Avanto, Espree [Siemens Healthcare], or GE Signa HDxt, Disc [GE Medical Systems]) MRI systems was acquired. Conventional T2w sequences have proven to be a dependable method for assessing lesion characteristics, demonstrating an intraobserver coefficient of variation (CoV) with an average of 2.31% during the acute phase. Notably, this percentage is lower than the intraobserver CoV reported by Huber et al. (4.3%) [13] and Pfyffer et al. (5.3%) [10]. Furthermore, these sequences exhibit robust inter-rater reliability, as evidenced by an intraclass correlation coefficient ($ICC_{2,1}$) of 0.9 [14]. In addition to its reliability, conventional T2w imaging has demonstrated associations with various clinical parameters. It has been linked to walking ability [14, 15] and clinical recovery outcomes [10, 13, 16–18].

Supralesional MRI acquisitions for the follow-ups at 1–12 months were performed with a 3-T Magnetom Verio (Siemens Healthcare). For the follow-ups at 24 and 60 months, the magnetic resonance (MR) system was upgraded to a 3T Magnetom Skyra^fit (Siemens Healthcare). For imaging the brain and spinal cord (C1–C3), we utilized a 16-channel radiofrequency (RF) receiver head and neck coil. The imaging protocol involved a three-dimensional (3D) high-resolution T1w magnetization-prepared rapid acquisition gradient echo (MPRAGE) sequence, widely recognized for assessing volumetric changes indicative of neurodegeneration [3, 7, 19–23]. In addition, we employed a multiparametric mapping protocol (MPM) [24] to investigate microstructural alterations, including myelin (MT_{sat}) [5, 6] and iron (R2*) [5]. These alterations have been demonstrated to occur post-SCI due to mechanisms such as inflammation, axonal degeneration, and demyelination [3, 20, 22]. Importantly, their assessment has shown an intersite bias below 5% in the brain [25] and below 12% in the spinal cord [26]. Both MR sequences shared the following parameters: 1 mm^3 isotropic resolution; 176 sagittal partitions; field of view, 224 × 256 mm^2. The further parameters of MPRAGE were: repetition time (TR), 2420 ms; echo time, 4.18 ms; inversion time, 960 ms; flip angle, 9°; and readout bandwidth, 150 Hz/pixel. The MPM protocol comprised three 3D multi-echo spoiled gradient echo sequences with distinct contrast weightings. The number of acquired bipolar echoes, flip angle, and TR for the proton

TABLE 1 Patient information.

ID	Age at injury, years	Sex	Initial AIS grade	Level of intramedullary lesion	Injury mechanism	Time to surgery	Type	Days of hospital-ization	UEMS baseline/outcome	LEMS baseline/outcome	SCIM baseline/outcome	LT baseline/outcome	PP baseline/outcome	Occupational therapy, h	Physiotherapy, h
1	30	M	A	C5/6	Dislocation fracture C5/6 & burst fracture C6	3 days	Fall	243	20/26	0/0	17/44	22/27	19/17	153	500
2	28	M	A	C4/5	Dislocation fracture C4/5	1 day	Fall	290	15/12	0/0	10/24	14/18	14/14	216	246
3	19	M	A	C5/7	Burst fracture C6	1 day	Fall	230	20/24	0/0	4/22	24/30	26/24	156	369
4	42	M	A	C6/7	Anterolisthesis of C6 relative to C7	1 day	Fall	277	23/24	0/0	18/41	27/20	20/13	145	321
5	20	M	A	C5/6	Dislocation fracture C5/6	1 day	MVA	292	21/21	0/0	4/39	21/45	19/18	168	327.5
6	32	M	A	C6/7	Flexion-distraction C5–C7	1 day	MVA	257	24/44	0/0	10/29	26/54	24/37	126	286
7	29	M	A	–[a]	Flexion-distraction T12/L1 & burst fracture L1	1 day	Fall	133	50/50	10/20	52/68	86/86	88/86	31	156
8	72	F	A	T10/12	Spinal epidural hematoma	1 day	Fall	195	50/50	0/0	48/39	75/74	77/68	69	99
9	52	M	B	C6/7	Dislocation fracture C6/7	1 day	MVA	240	26/39	0/31	16/29	65/61	38/58	95	223
10	23	M	B	C6/7	Dislocation fracture C6/7	1 day	Fall	217	42/50	0/25	24/70	69/77	38/33	87	301
11	71	M	B	C7	Flexion-distraction fracture C6/7	3 days	Fall	256	36/48	16/42	17/43	85/66	36/25	132	366
12	30	M	B	C6/7	Dislocation fracture C6/7	1 day	MVA	190	38/47	0/0	38/59	64/65	35/52	84	201
13	67	F	B	T6/12	Congestive myelopathy T6–T12	5 days	spon.	249	50/50	2/37	41/30	78/87	75/90	86	603
14	53	F	C	C4/5	Spinal compression C4/5	2 days	Fall	159	16/42	36/49	15/84	62/62	53/94	90	99
15	31	M	C	T2/7	Dislocation fracture T4/5	3 days	Fall	105	50/50	9/50	40/96	79/112	58/84	25	90
16	71	M	C	T10/12	Vascular infarction	3 days	spon.	164	50/50	43/50	47/69	88/93	43/50	46	182
17	68	M	D	C3/4	Spinal compression C3/4	1 day	Fall	55	48/50	48/50	100/99	60/112	52/99	10	10
18	47	M	D	C6/7	Dislocation fracture C6/7	5 days	MVA	42	35/44	46/42	99/98	104/98	104/84	5	3
19	71	F	D	T6/8	Spinal compression T3–T9	–	spon.	38	50/50	43/50	56/97	83/112	81/112	8	13
20	46	F	D	T6/12	Prolapsed disk T8/9 with spinal ischemia	–	spon.	76	50/50	45/49	65/96	84/91	74/99	3	15
21	52	M	D	–[a]	Flexion-distraction T9/10	1 day	Fall	48	50/50	48/49	84/100	95/94	89/90	8	39
22	77	F	D	T9/conus medullaris	Aortic embolism with spinal ischemia	–	spon.	77	50/50	34/47	30/75	96/95	70/88	25	74
23	44	M	D	None	Herniated disk L3–L4	1 day	Fall	77	50/50	39/45	84/100	107/106	109/98	11	57

Abbreviations: AIS, ASIA Impairment Scale; C, cervical level; F, female; L, lumbar level; LEMS, lower extremity motor score; LT, light touch score; M, male; MVA, motor vehicle accident; PP, pin prick score; SCIM, Spinal Cord Independence Measure; spon., spontaneous; T, thoracic level; UEMS, upper extremity motor score.

[a]Spinal cord cannot be assessed at the level of injury due to artefacts caused by a metal implant.

density-weighted, T1w, and magnetization transfer (MT)-weighted sequences were 8/4°/25 ms, 8/23°/25 ms, and 6/9°/37 ms, respectively, with an echo spacing of 2.46 ms. MT weighting was achieved by an off-resonance RF pulse prior to nonselective excitation and a readout bandwidth of 488 Hz/pixel.

The hMRI toolbox (version 0.2.0) [27] was used to estimate quantitative maps of MT_{sat}, using UNICORT to correct for residual B1+ residual effects of the MT_{sat} maps [28], and R2*.

Tensor-based morphometry [29] was used to analyse volume changes over time. To analyse—at the voxel level—the brain and C1–C3 simultaneously, the statistical parametric mapping brain-spinal cord template (SPM-BSC) method was chosen [4]. MPRAGE images were first aligned with the T1w Montreal Neurological Institute template [27]. Second, images of each subject were longitudinally coregistered [29], furnishing an intensity bias-free average image of each individual, including deformation field, and Jacobian determinants maps [29]. Third, the average image was segmented [30] using the brain–neck template [4]. To assess morphological changes in the spinal cord, the native-space GM and WM tissue maps were combined to form a neural tissue (NT) probability map. For the analysis of SPM-BSC data, a group-specific spinal cord mask was computed by thresholding the average of the NT maps of all participants to include voxels with probability of >50% and further restricting this mask to the spinal cord at levels C1–C3 (visually defined) [31]. Fourth, the Dartel algorithm was applied for spatial normalization. Fifth, the Jacobian determinant was used to modulate the midpoint average GM, WM, and NT maps. Finally, GM and WM maps were smoothed with a 6-mm full width at half maximum (FWHM) Gaussian kernel. For MT_{sat} and R2*, a tissue-specific smoothing procedure [27] with a Gaussian kernel of 3-mm FWHM was used. In the spinal cord (i.e., NT map), no smoothing was applied, due to its small size and the lack of gyrification, thereby increasing specificity and reducing the number of false positives [32].

The three regions of interest (ROIs) were (i) C1–C3, (ii) cranial corticospinal tracts (CST), and (iii) sensorimotor cortices (M1/S1). The M1/S1 and CST were defined using the anatomy [33] and suite toolbox [34].

To track lesion changes, the intramedullary lesion area (IMLA), lesion length (IMLL), and tissue bridges (TB) were manually segmented on the midsagittal slice of the T2w image with Jim software (version 7.0, Xinapse Systems) [14]. Lesions of two subjects could not be segmented due to metal implants artefacts. As a complementary verification, we also assessed the cross-sectional cord area at the C2–C3 level using Jim (Figure S1.2).

Statistical analysis

For assessing recovery, linear mixed effect models were used in RStudio (version 3.6.0) with clinical measures as the response variable and (log-transformed) time as the independent variable, to accommodate nonlinear recovery trajectories. Random intercept, random slope, age, and sex were included as covariates of no interest for each subject. Results with $p < 0.05$ (Bonferroni corrected) were considered statistically significant.

For lesion changes, repeated measures analysis of variance was performed to compare the effect of time on the lesion. Post hoc paired t-tests were conducted to assess changes within the first month and subsequent changes over 5 years. Results with $p < 0.05$ (Bonferroni corrected) were considered statistically significant.

The Sandwich Estimator Toolbox (version 2.1.0) [35] was used to assess longitudinal volume changes and microstructural changes within the previously defined ROIs. The general linear model (GLM) included a group indicator, time, and quadratic effect of time. Age and sex were included as covariates of no interest to preclude potential confounds. A one-tailed t-test was used to compare potential differences between both groups. For the 1-month time point difference analysis, time variables were adjusted to the 1-month scan as reference point (i.e., assigned a value of 0), allowing intercept analysis. Participants having fewer than three scans were excluded from the analysis (MPRAGE = 1, MPM = 2). For the C1–C3 analysis, additionally one participant was excluded due to inaccurate spinal normalization. Results with $p < 0.05$ topological false discovery rate-corrected [36] were considered statistically significant.

For the association between changes in TB within the first month (delta TB between 3 days and 1 month) and volumetric and microstructural rate changes over 5 years, the TB changes were added to the GLM described above, and the neurological level of injury as a variable of no interest. For the association between structural changes over 5 years and recovery, each subject's last and baseline motor or SCIM score were included. For the association between patients' relative recovery and TB changes or mean value of the statistically significant baseline differences (i.e., significant intercept

FIGURE 1 Time course of lesion characteristics and clinical recovery. (a) Representative serial midsagittal T2-weighted scans showing the evolution of the focal lesion over 5 years. The lesion edge is outlined and the midsagittal total tissue bridges (TB) width (TB = dorsal + ventral tissue bridges), intramedullary lesion area (IMLA), and intramedullary lesion length (IMLL) are indicated. Individual trajectories of patients' midsagittal tissue bridges, IMLA, and IMLL changes over 5 years are shown. Note the rapid changes within the first month, followed by only marginal changes in the next years. (b) Recovery trajectories of the International Standards for Neurological Classification of Spinal Cord Injury (ISNCSCI) motor score and of the Spinal Cord Independence Measure (SCIM) scores. (c) Scatterplot showing the association between midsagittal TB changes within the first months (1-month TB – hyperacute TB) and relative motor score recovery and the association between relative baseline spinal cord volume (i.e., neural tissue average within C1–C3 [percent units (p.u.)]) and the relative motor score recovery. In panels a and b, in red, the mean and standard error are depicted, and red dashed lines show individual longitudinal data for patients. In panels a–c, dark red indicates subjects with nontraumatic spinal cord injury.
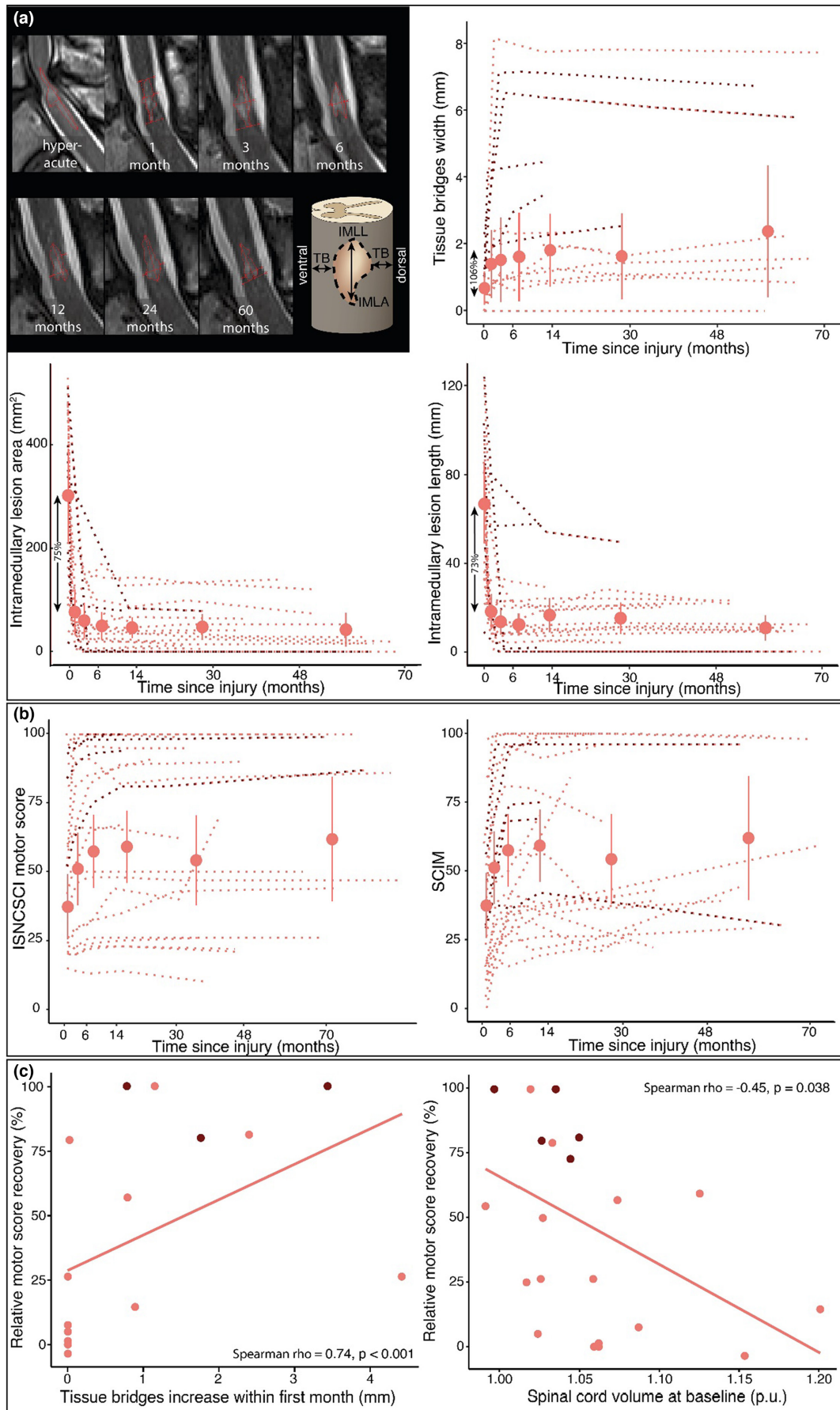
differences between healthy controls and SCI patients), a Spearman rank correlation was conducted.

RESULTS

We recruited 21 healthy controls (33.7 ± 9.8 years old) and 23 SCI patients with an acute SCI (mean age $\pm$ SD $= 46.7 \pm 19.1$ years). Of those, 13 were tetraplegic (36.8 ± 19.8 years) and 10 were paraplegic (56.0 ± 17.9 years; Table 1). SCI patients were scanned on average at 3.3 days postinjury (median $\pm$ interquartile range [first and third quantile] $= 2 \pm 2$ [1–3] days) and at 1-month (1 ± 1 [1–2] months), 3-month (3 ± 1 [3–4] months), 6-month (6 ± 2 [6–8] months), 12-month (12 ± 1 [12–13] months), 24-month (26 ± 5 [24–29] months), and 60-month (60 ± 13 [52–70] months) follow-ups. The adherence to the study protocol was 94% for controls and 85% for patients. Over the 5-year study period, patients' motor scores recovered by a total of 12.86 points ($p < 0.001$, 95% confidence interval [CI] $= 6.70$–19.00), of which in the first year 7.25 points, from 1 year to 2 years 2.42 points, and from 2 years to 5 years 3.19 points were recovered. Over 5 years, patients' SCIM scores recovered by a total of 26.08 points ($p < 0.001$, 95% CI $= 17.00$–35.20), of which in the first year 14.7 points, from 1 year to 2 years 4.9 points, and from 2 years to 5 years 6.48 points were recovered.

At 3 days post-SCI, the width of TB was on average 0.68 mm (95% CI $= 0.18$–1.19 mm). TB became more clearly defined at the end of the first month (1.41 mm, 95% CI $= 0.39$–2.43 mm, $p = 0.02$) and changed marginally between 1 month and 5 years ($p = 0.18$). At 3.3 days post-SCI, the mean IMLA and IMLL were 303 mm² (95% CI $= 213$–392 mm²), and 66.7 mm (95% CI $= 48.9$–84.5 mm), respectively. IMLA and IMLL decreased within the first month by 75% and 73% to 77 mm² (95% CI $= 33$–121 mm², $p < 0.001$) and 18.0 mm (95% CI $= 10.0$–26.0 mm, $p < 0.001$), respectively. The IMLA and IMLL remained stable between 1 month and 5 years (IMLA, $p = 0.28$, IMLL, $p = 0.30$; Figure 1, Table S1.1).

Over the first 4 weeks post-SCI, SCI patients, compared to healthy controls, showed an increased volume of the C1–C3 (i.e., NT map) and intracranial CST (i.e., swelling at baseline), accompanied by increased iron-sensitive R2* along the lateral C1–C3 and decreased myelin-sensitive MT$_{sat}$ within the dorsal C1–C3 (Figure 2, Tables S1.2–S1.4). Also, during this early period, volume and MT$_{sat}$ decreases were observed in the bilateral M1/S1 (Figure 2, Table S1.3). Over 5 years, the rate of cord volume (i.e., NT map) decrease decelerated, whereas intracranial CST volume showed no sign of deceleration (Figure 2, Figure S1.2, Tables S1.2, and S1.4). At C1–C3, MT$_{sat}$ decreased but slowed deceleration between 2 and 5 years (Figure 2, Table S1.3). In the M1/S1, atrophy was already evident at 1 month but showed no further changes over time.

Greater TB changes within the first month were associated with less intracranial CST volume increase, less GM volume loss within the right M1/S1 after 1 month, slower rates of volume loss in the C1–C3 (i.e., NT map) and CST, and slower MT$_{sat}$ decline in the C1–C3 over 5 years (Figure 3, Tables S1.2 and S1.3).

TB increase within the first month was positively associated with motor score recovery ($n = 16$, $\rho = 0.74$, $p < 0.001$; Figure 1c). Less C1–C3 atrophy over 5 years was associated with improved baseline-adjusted motor score after 5 years (Figure 4, Table S1.2). Spinal cord swelling (i.e., increased NT map average within C1–C3 relative to healthy controls) at 1 month was negatively associated with motor score recovery ($n = 22$, $\rho = -0.45$, $p = 0.04$; Figure 1c). A smaller MT$_{sat}$ decrease of the C1–C3 over 5 years was associated with a better baseline-adjusted motor and SCIM score over 5 years (Figure 4, Table S1.3). Less R2* increase in the M1/S1 over 5 years was associated with better baseline-adjusted SCIM score over 5 years (Figure 4, Table S1.3). An improved baseline-adjusted motor and SCIM score was associated with decreased C1–C3 volume change (i.e., NT map; Figure 4, Table S1.3).

DISCUSSION

This study shows that the spinal lesion undergoes rapid changes within the first days and weeks following SCI. These early lesion changes are associated with both remote degeneration and clinical recovery. Remote changes continue for at least 5 years. Crucially, this study provides a unique long-term characterization of the interaction between lesion extent, its early dynamics, and association with remote neurodegenerative and compensatory microstructural changes within the C1–C3 and brain over 5 years. This study has revealed a number of new findings that we will discuss in more detail under the four aims of the study.

Previous studies have primarily assessed the predictive value of the matured lesion at 1 month post-SCI for neurologic recovery [10]. Here, we tracked the evolution of the lesion characteristics within the first 72 h and documented a rapid resolution of the perilesional cord oedema within the first month post-SCI. Starting from the earliest time point after SCI (3 days post-SCI), the spinal cord lesion showed a reduction in size by more than two thirds, revealing demarcations of the TB. Crucially, the extent of the lesion—including TB—remains stable from 1 month to at least 5 years post-SCI. This suggests that potential treatments—targeting the protection and repair of the injured spinal cord—should be administrated as early as possible.

These rapid lesion changes were associated with remote swelling, a feature commonly associated with neuroinflammation [1, 37]. Specifically, the C1–C3 and intracranial CST showed increased volume (i.e., swollen) by approximately 5% and 3%, respectively. This volume increase was paralleled by signs of increased iron accumulation (i.e., R2* $= 18\%$) and demyelination (i.e., MT$_{sat} = 2\%$). The latter processes are both implicated in neurodegenerative and neuroinflammatory processes [38]. Interestingly, within the following months, the initial swelling of the C1–C3 and intracranial CST turned into a net loss of volume (i.e., C1–C3 $= 9\%$, CST $= 2\%$) and was accompanied by microstructural alterations (i.e., MT$_{sat}$). In the ensuing 5 years, the intracranial CST and M1/S1—which were already undergoing progressive changes within the first 2 years post-SCI
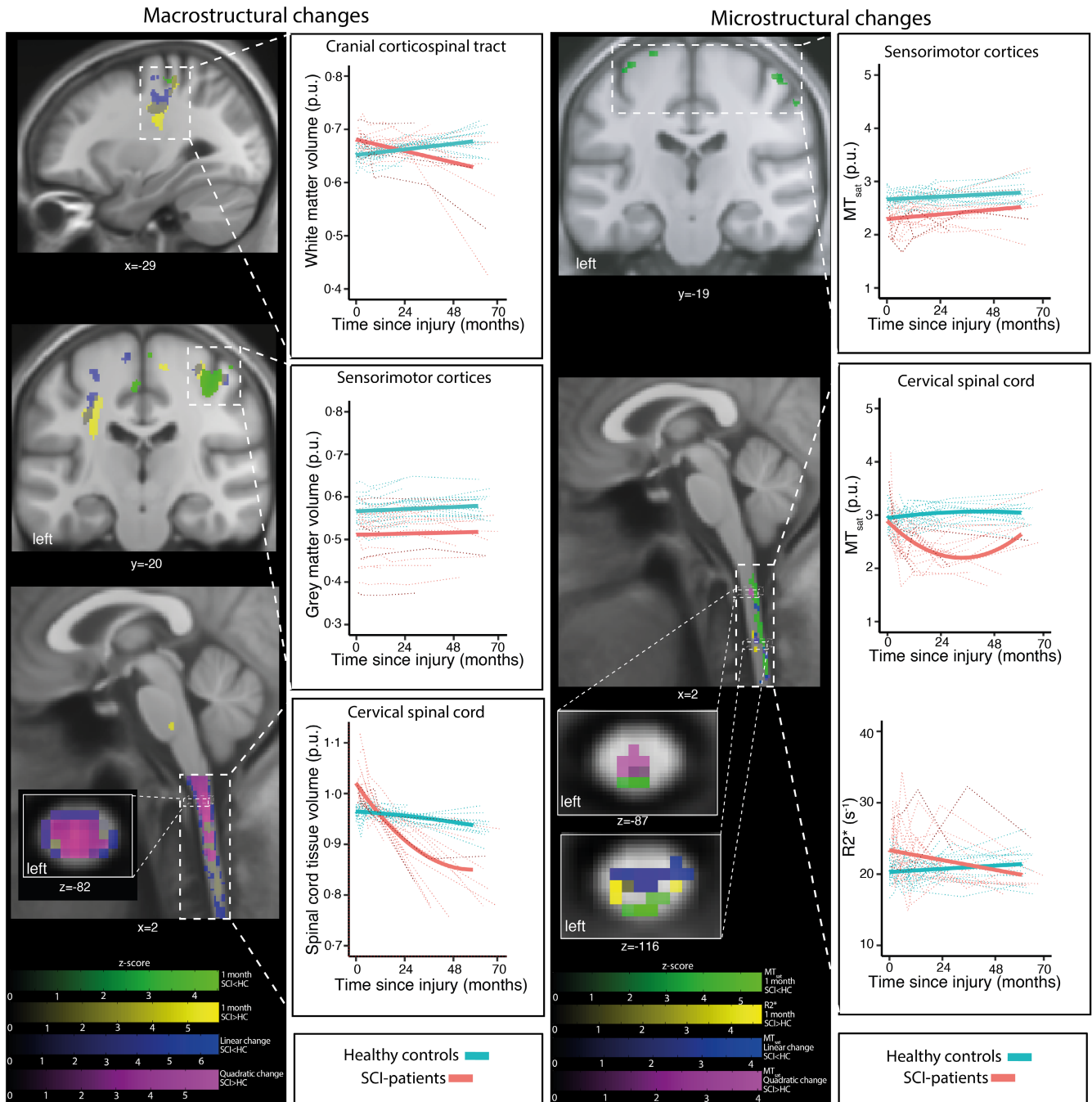
FIGURE 2 Cervical spinal cord and brain structural changes. Overlay of statistical parametric maps (significant clusters $p < 0.05$ false discovery rate-corrected, cluster size ≥ 20) and time courses (for illustrative purposes) shows morphometric (left column) and microstructural (right column) changes of spinal cord injured patients (SCI-patients) compared to healthy controls (HC) from baseline up to >5 years. For the macrostructural changes, the significant 1-month volume decrease in SCI-patients is shown in green, 1-month volume increase of SCI-patients in yellow, longitudinal linear volume decrease in blue, and deceleration of linear volume decrease in magenta. For the microstructural changes (i.e., effective transverse relaxation rate [R2*] and magnetization transfer saturation [MT_{sat}]), significant 1-month MT_{sat} decrease in SCI-patients is shown in green, 1-month R2* increase in SCI-patients in yellow, longitudinal linear MT_{sat} decrease in blue, and deceleration of linear MT_{sat} decrease in SCI-patients in magenta. Corresponding (for illustrative purposes) macrostructural and microstructural trajectories are shown for local effects in voxel-based morphometry and voxel-based quantification with healthy controls in blue and SCI-patients in red. The bold solid lines depict the model average of the significant cluster, and the dotted lines represent the raw individual trajectory average of the significant cluster. Dark red indicates subjects with nontraumatic spinal cord injury. p.u., percent units.
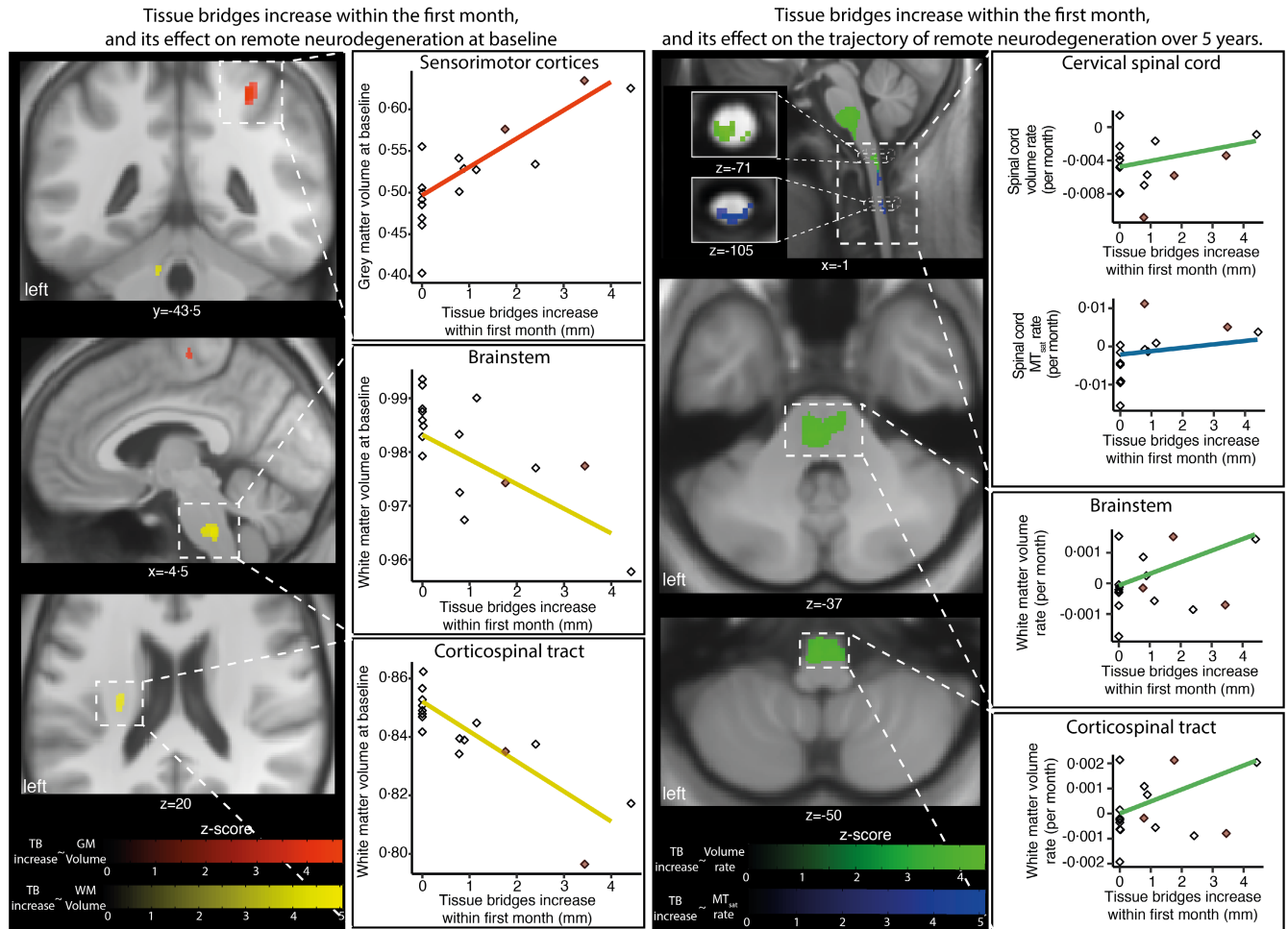
FIGURE 3 Impact of early lesion dynamics on remote neurodegeneration. Overlay of statistical parametric maps (significant clusters $p < 0.05$ false discovery rate-corrected) shows the correlation between baseline values in volume or magnetization transfer saturation (MT_{sat}) metrics (left column) and rates of change over 5 years (right column) with tissue bridges (TB) width increases within the first month (1-month TB – 3-day TB). The association between grey matter volume decrease at baseline and TB width increase within the first month is depicted in red. The association between white matter volume increase at baseline and TB width increase within the first month is shown in yellow. The correlation between linear volume rate over 5 years and TB width increase within the first month is depicted in green. The correlation between linear MT_{sat} rate over 5 years and TB width increase within the first month is shown in blue. Corresponding (for illustrative purposes) scatterplots show macrostructural and microstructural baseline values (left column) and linear rates (right column) over 5 years and TB width increase within the first month per subject, with bold solid lines representing the model average of the significant cluster. Dark red indicates subjects with nontraumatic spinal cord injury.

[3]—continued this pattern, without evidence of slowing down over 5 years, whereas the spinal cord showed signs of deceleration.

More extensive spinal cord lesions are associated with remote neuroinflammatory and neurodegenerative processes across the motor system for at least 5 years. Interestingly, the extent of TB early after injury is associated with remote degenerative changes after 1 month and their rate of change over the subsequent 5 years. Patients with anatomical complete lesions (i.e., no TB) show the greatest degenerative changes above the level of injury, where C1–C3 volume decreased by 16% and C1–C3 MT_{sat} reduced by 15% over 5 years. This ongoing degeneration has been shown in both animal models of SCI and in human spinal cord specimens [39]. In contrast, SCI patients with preserved TB had at least a 25% reduction in the rate of C1–C3 atrophy and showed an increase

of 11% in MT_{sat} content over 5 years when compared to baseline. This progressive character of supralesional neurodegeneration detected by MRI speaks to the systemic response following an isolated injury to the spinal cord. Therefore, remote and enduring degeneration might contribute to functional and cognitive decline, which occurs in some patients with SCI [40], similar to that found in traumatic brain injury [41].

Both lesion changes and remote degeneration were shown to be associated with recovery. SCI patients without—or with small—TB within the first month showed, on average, a relative motor score recovery of 5%, and subjects with an increase in TB within the first month showed a relative motor score recovery of 71%. This finding is in support of previous reports in which the extent of TB at 1 month post-SCI is associated with tract-specific
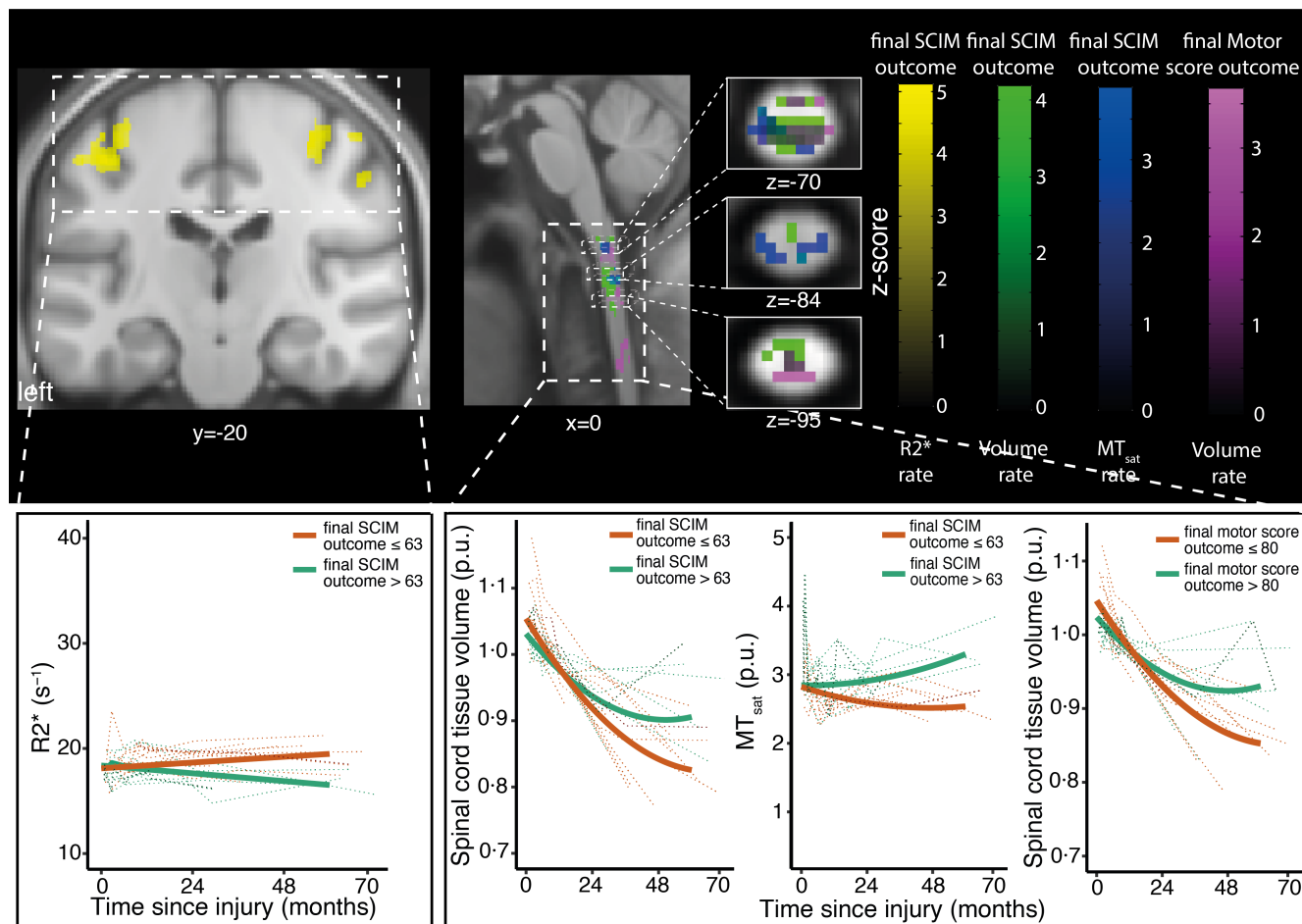
FIGURE 4 Associations between structural changes and clinical recovery. Upper row: Overlay of statistical parametric maps (significant clusters $p < 0.05$ false discovery rate-corrected corrected) shows the association between rates of change in volumetric (green) or magnetization transfer saturation (MT_{sat}; blue) and effective transverse relaxation rate (R2*; yellow) metrics with clinical outcome over 5 years (i.e., Spinal Cord Independence Measure [SCIM] and International Standards for Neurological Classification of Spinal Cord Injury motor score). The lower row illustrates differences in the rates between patients with a better final outcome (upper median of the final SCIM [>63 points] and motor scores [>80 points], green) and patients with a worse final outcome (lower median of the final SCIM [≤63 points] and motor scores [≤80 points], red). The bold solid lines depict the fitted model average of the significant cluster for the two groups with better or worse final clinical outcomes, and the dotted lines represent the raw individual trajectory average of the significant cluster. Dark red and dark green represent subjects with nontraumatic spinal cord injury. p.u., percent units.

recovery and electrophysiological readouts [42]. Further up, less swelling and less myelin-sensitive MT_{sat} reduction in the C1–C3 was associated with better motor recovery over 5 years. The clinical sequelae of these MRI changes suggests that swelling might be a direct correlate to inflammation and demyelination that occurs post-SCI [43]. Inflammation is known to reduce the integrity of axons, hence impeding electrophysiological message passing along their projections. Therefore, a rapid decrease in swelling and fewer demyelinating fibres could promote recovery. This notion goes in line with the findings that in the cortical GM of the motor cortices, less iron-sensitive R2* accumulation was associated with a better SCIM over 5 years. Interestingly, in addition to acute structural changes being related to outcome, lower atrophy rates in the C1–C3 were also associated with a better motor and functional independence outcome over 5 years. The identification

of spatiotemporal trajectories of neurodegeneration, following acute SCI, may enable more specific treatment strategies.

This study has some limitations. Although there is strong histological evidence that both MT_{sat} and R2* are sensitive to myelin and iron content [5, 6], they are only indirect markers with limited specificity. Thus, we cannot exclude a partial contribution of unexplored physiologic/cellular processes, and the results need to be interpreted in conjunction with histological studies of SCI. The standard MRI for evaluating lesion parameters was acquired on average 3.3 days after injury, whereas the brain and C1–C3 MRI was acquired about 1 month post-SCI. Nevertheless, this delay still allowed us to assess rather early remote changes. However, we could not assess the peak of the swelling, which happened within the first month. Furthermore, it should be noted that we investigated the spatiotemporal dynamics of tissue-specific neurodegeneration in

the spinal cord above and below the site of SCI in a separate cohort [44]. Another potential confound is scanner upgrade. However, this effect could be minimized by the study design, as both controls and patients were scanned in the same time period, before and after the upgrade. Therefore, both cohorts are equally affected, providing reliable statistical analyses. The MPM protocol showed good repeatability between different scanners, allowing for multicenter clinical trials [25, 26]. Thus, only minimal effects of the scanner upgrade on quantitative maps are expected [25, 26]. For the lesion parameters, it has not been demonstrated that variations in scanner vendors or field strengths have a strong influence [10, 17, 18, 45]. It is worth mentioning that traumatic and nontraumatic causes of SCI were included. However, it was shown that the focal lesion and the clinical outcome are not significantly different between both etiologies [10, 46].

In conclusion, this study shows that hyperacute lesion changes are associated with remote and progressive neuroinflammatory and neurodegenerative changes in the C1–C3 and brain up to 5 years post-SCI. Surprisingly, local lesion changes subside within 1 month post-SCI, but persist supralesionally. These distinct spatiotemporal trajectories of neurodegenerative changes provide windows of opportunities for targeted treatment within the acute and chronic phase of injury. Consequently, treatment trials for acute SCI could target local lesion changes, and trials for chronic SCI could include neuroprotective as well as anti-inflammatory strategies [43] to prevent or slow down remote degeneration. Tracking remote degenerative changes and their associations with lesion characteristics—and clinical status—provides valuable insights, which might open new avenues to understand better the complex interplay between different pathophysiological mechanisms following SCI.

AUTHOR CONTRIBUTIONS

Tim M. Emmenegger: Methodology; analysis; editing draft. **Dario Pfyffer:** Methodology; editing draft. **Armin Curt**: Conceptualization; methodology; editing draft. **Simon Schading-Sassenhausen:** Conceptualization; methodology; analysis; editing draft. **Markus Hupp:** Methodology; editing draft. **John Ashburner**: Conceptualization; methodology; editing draft. **Karl Friston**: Conceptualization; methodology; editing draft. **Nikolaus Weiskopf:** Conceptualization; methodology; editing draft. **Alan Thompson**: Conceptualization; methodology; analysis; editing draft. **Patrick Freund**: Conceptualization; methodology; analysis; editing draft.

ACKNOWLEDGEMENTS

FUNDING INFORMATION

CONFLICT OF INTEREST STATEMENT

N.W. holds a patent on acquisition of MRI data during spoiler gradients (US 10,401,453 B2), which were parts of sequences used in this study. N.W. was a speaker at an event organized by Siemens Healthcare, which was the scanner brand used in this study, and was reimbursed for the travel expenses. The Max Planck Institute for Human Cognitive and Brain Sciences and Wellcome Centre for Human Neuroimaging have institutional research agreements with Siemens Healthcare, which as previously mentioned was the scanner brand used in this study.

DATA AVAILABILITY STATEMENT

The data that support the findings of this study are available on request from the corresponding author. The data are not publicly available due to privacy or ethical restrictions.

ORCID

Tim M. Emmenegger https://orcid.org/0000-0003-0350-3482
Dario Pfyffer https://orcid.org/0000-0002-2406-9251

REFERENCES

1. Ahuja CS, Wilson JR, Nori S, et al. Traumatic spinal cord injury. *Nat Rev Dis Prim*. 2017;3:17018. doi:10.1038/nrdp.2017.18
2. Freund P, Seif M, Weiskopf N, et al. MRI in traumatic spinal cord injury: from clinical assessment to neuroimaging biomarkers. *Lancet Neurol*. 2019;18(12):1123-1135. doi:10.1016/S1474-4422(19)30138-3
3. Ziegler G, Grabher P, Thompson A, et al. Progressive neurodegeneration following spinal cord injury: implications for clinical trials. *Neurology*. 2018;90(14):e1257-e1266. doi:10.1212/WNL.0000000000005258
4. Freund P, Papinutto N, Bischof A, et al. Simultaneous assessment of regional distributions of atrophy across the neuraxis in MS patients. *NeuroImage Clin*. 2022;34(March):102985. doi:10.1016/j.nicl.2022.102985
5. Weiskopf N, Edwards LJ, Helms G, Mohammadi S, Kirilina E. Quantitative magnetic resonance imaging of brain anatomy and in vivo histology. *Nat Rev Phys*. 2021;3(8):570-588. doi:10.1038/s42254-021-00326-1
6. Georgiadis M, Schroeter A, Gao Z, et al. Nanostructure-specific X-ray tomography reveals myelin levels, integrity and axon orientations in mouse and human nervous tissue. *Nat Commun*. 2021;12(1):2941. doi:10.1038/s41467-021-22719-7
7. Grabher P, Callaghan MF, Ashburner J, et al. Tracking sensory system atrophy and outcome prediction in spinal cord injury. *Ann Neurol*. 2015;78(5):751-761. doi:10.1002/ana.24508
8. Kirshblum SC, Waring W, Biering-Sorensen F, et al. Reference for the 2011 revision of the international standards for neurological

classification of spinal cord injury. *J Spinal Cord Med.* 2011;34(6):547-554. doi:10.1179/107902611X13186000420242

9. Catz MI, Flavia SA. The Catz-Itzkovich SCIM: a revised version of the Spinal Cord Independence Measure. *Disabil Rehabil.* 2001;23(6):263-268. doi:10.1080/096382801750110919

10. Pfyffer D, Huber E, Sutter R, Curt A, Freund P. Tissue bridges predict recovery after traumatic and ischemic thoracic spinal cord injury. *Neurology.* 2019;93(16):e1550-e1560. doi:10.1212/WNL.0000000000008318

11. Scivoletto G, Laurenza L, Mammone A, Foti C, Molinari M. Recovery following ischemic myelopathies and traumatic spinal cord lesions. *Spinal Cord.* 2011;49(8):897-902. doi:10.1038/sc.2011.31

12. Iseli E, Cavigelli A, Dietz V, Curt A. Prognosis and recovery in ischaemic and traumatic spinal cord injury: clinical and electrophysiological evaluation. *J Neurol Neurosurg Psychiatry.* 1999;67(5):567-571. doi:10.1136/jnnp.67.5.567

13. Huber E, Lachappelle P, Sutter R, Curt A, Freund P. Are midsagittal tissue bridges predictive of outcome after cervical spinal cord injury? *Ann Neurol.* 2017;81(5):740-748. doi:10.1002/ana.24932

14. O'Dell DR, Weber KA, Berliner JC, et al. Midsagittal tissue bridges are associated with walking ability in incomplete spinal cord injury: a magnetic resonance imaging case series. *J Spinal Cord Med.* 2020;43(2):268-271. doi:10.1080/10790268.2018.1527079

15. Berliner JC, O'Dell DR, Albin SR, et al. The influence of conventional T 2 MRI indices in predicting who will walk outside one year after spinal cord injury. *J Spinal Cord Med.* 2023;46(3):501-507. doi:10.1080/10790268.2021.1907676

16. Vallotton K, Huber E, Sutter R, Curt A, Hupp M, Freund P. Width and neurophysiologic properties of tissue bridges predict recovery after cervical injury. *Neurology.* 2019;92(24):e2793-e2802. doi:10.1212/WNL.0000000000007642

17. Pfyffer D, Vallotton K, Curt A, Freund P. Tissue bridges predict neuropathic pain emergence after spinal cord injury. *J Neurol Neurosurg Psychiatry.* 2020;91(10):1111-1117. doi:10.1136/jnnp-2020-323150

18. Pfyffer D, Vallotton K, Curt A, Freund P. Predictive value of midsagittal tissue bridges on functional recovery after spinal cord injury. *Neurorehabil Neural Repair.* 2021;35(1):33-43. doi:10.1177/1545968320971787

19. Freund P, Wheeler-Kingshott CA, Nagy Z, et al. Axonal integrity predicts cortical reorganisation following cervical injury. *J Neurol Neurosurg Psychiatry.* 2012;83(6):629-637. doi:10.1136/jnnp-2011-301875

20. Seif M, Gandini Wheeler-Kingshott CA, Cohen-Adad J, Flanders AE, Freund P. Guidelines for the conduct of clinical trials in spinal cord injury: neuroimaging biomarkers. *Spinal Cord.* 2019;57(9):717-728. doi:10.1038/s41393-019-0309-x

21. Freund P, Friston K, Thompson AJAJ, et al. Embodied neurology: an integrative framework for neurological disorders. *Brain.* 2016;139(6):1855-1861. doi:10.1093/brain/aww076

22. Freund P, Weiskopf N, Ashburner J, et al. MRI investigation of the sensorimotor cortex and the corticospinal tract after acute spinal cord injury: a prospective longitudinal study. *Lancet Neurol.* 2013;12(9):873-881. doi:10.1016/S1474-4422(13)70146-7

23. Freund P, Weiskopf N, Ward NS, et al. Disability, atrophy and cortical reorganization following spinal cord injury. *Brain.* 2011;134(6):1610-1622. doi:10.1093/brain/awr093

24. Weiskopf N, Suckling J, Williams G, et al. Quantitative multi-parameter mapping of R1, PD(*), MT, and R2(*) at 3T: a multi-center validation. *Front Neurosci.* 2013;7:1-11. doi:10.3389/fnins.2013.00095

25. Leutritz T, Seif M, Helms G, et al. Multiparameter mapping of relaxation (R1, R2*), proton density and magnetization transfer saturation at 3 T: a multicenter dual-vendor reproducibility and repeatability study. *Hum Brain Mapp.* 2020;41(15):4232-4247. doi:10.1002/hbm.25122

26. Seif M, Leutritz T, Schading S, et al. Reliability of multi-parameter mapping (MPM) in the cervical cord: a multi-center multi-vendor quantitative MRI study. *Neuroimage.* 2022;264(August):119751. doi:10.1016/j.neuroimage.2022.119751

27. Tabelow K, Balteau E, Ashburner J, et al. hMRI—a toolbox for quantitative MRI in neuroscience and clinical research. *Neuroimage.* 2019;194:191-210. doi:10.1016/j.neuroimage.2019.01.029

28. Emmenegger TM, David G, Ashtarayeh M, et al. The influence of radio-frequency transmit field inhomogeneities on the accuracy of G-ratio weighted imaging. *Front Neurosci.* 2021;15:1-17. doi:10.3389/fnins.2021.674719

29. Ashburner J. Symmetric diffeomorphic modeling of longitudinal structural MRI. *Front Neurosci.* 2013;6:197. doi:10.3389/fnins.2012.00197

30. Ashburner J, Friston KJ. Unified segmentation. *Neuroimage.* 2005;26(3):839-851. doi:10.1016/j.neuroimage.2005.02.018

31. Azzarito M, Kyathanahally SP, Balbastre Y, et al. Simultaneous voxel-wise analysis of brain and spinal cord morphometry and microstructure within the SPM framework. *Hum Brain Mapp.* 2020;42:220-232. doi:10.1002/hbm.25218

32. Nichols TE. Multiple testing corrections, nonparametric methods, and random field theory. *Neuroimage.* 2012;62(2):811-815. doi:10.1016/j.neuroimage.2012.04.014

33. Eickhoff SB, Stephan KE, Mohlberg H, et al. A new SPM toolbox for combining probabilistic cytoarchitectonic maps and functional imaging data. *Neuroimage.* 2005;25(4):1325-1335. doi:10.1016/j.neuroimage.2004.12.034

34. Diedrichsen J. A spatially unbiased atlas template of the human cerebellum. *Neuroimage.* 2006;33(1):127-138. doi:10.1016/j.neuroimage.2006.05.056

35. Guillaume B, Hua X, Thompson PM, Waldorp L, Nichols TE, Alzheimer's Disease Neuroimaging Initiative. Fast and accurate modelling of longitudinal and repeated measures neuroimaging data. *Neuroimage.* 2014;94:287-302. doi:10.1016/j.neuroimage.2014.03.029

36. Chumbley J, Worsley K, Flandin G, Friston K. Topological FDR for neuroimaging. *Neuroimage.* 2010;49(4):3057-3064. doi:10.1016/j.neuroimage.2009.10.090

37. Hellenbrand DJ, Quinn CM, Piper ZJ, Morehouse CN, Fixel JA, Hanna AS. Inflammation after spinal cord injury: a review of the critical timeline of signaling cues and cellular infiltration. *J Neuroinflammation.* 2021;18(1):284. doi:10.1186/s12974-021-02337-2

38. Brennan FH, Li Y, Wang C, et al. Microglia coordinate cellular interactions during spinal cord repair in mice. *Nat Commun.* 2022;13(1):4096. doi:10.1038/s41467-022-31797-0

39. Buss A, Schwab ME. Sequential loss of myelin proteins during Wallerian degeneration in the rat spinal cord. *Glia.* 2003;42(4):424-432. doi:10.1002/glia.10220

40. Sachdeva R, Gao F, Chan CCH, Krassioukov AV. Cognitive function after spinal cord injury: a systematic review. *Neurology.* 2018;91(13):611-621. doi:10.1212/WNL.0000000000006244

41. Maas AIR, Menon DK, Adelson PD, et al. Traumatic brain injury: integrated approaches to improve prevention, clinical care, and research. *Lancet Neurol.* 2017;16(12):987-1048. doi:10.1016/S1474-4422(17)30371-X

42. Rink S, Pavlov S, Wöhler A, et al. Numbers of axons in spared neural tissue bridges but not their widths or areas correlate with functional recovery in spinal cord-injured rats. *J Neuropathol Exp Neurol.* 2020;79(11):1203-1217. doi:10.1093/jnen/nlaa050

43. Zrzavy T, Schwaiger C, Wimmer I, et al. Acute and non-resolving inflammation associate with oxidative injury after human spinal cord injury. *Brain.* 2021;144(1):144-161. doi:10.1093/brain/awaa360

44. David G, Pfyffer D, Vallotton K, et al. Longitudinal changes of spinal cord grey and white matter following spinal cord injury. *J Neurol Neurosurg Psychiatry.* 2021;92(11):1222-1230. doi:10.1136/jnnp-2021-326337

45. Pfyffer D, Huber E, Sutter R, et al. Are midsagittal tissue bridges predictive of outcome after cervical spinal cord injury? *Ann Neurol.* 2020;81(5):33-43. doi:10.1136/jnnp-2020-323150

46. Scivoletto G, Torre M, Mammone A, et al. Acute traumatic and ischemic spinal cord injuries have a comparable course of recovery. *Neurorehabil Neural Repair.* 2020;34(8):723-732. doi:10.1177/1545968320939569

SUPPORTING INFORMATION

Additional supporting information can be found online in the Supporting Information section at the end of this article.